

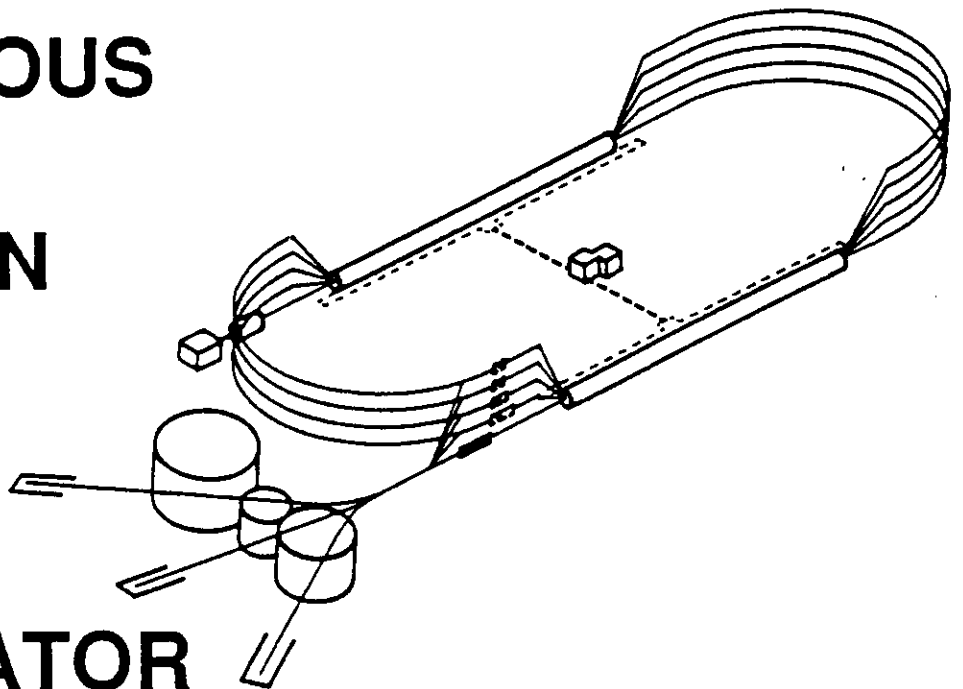
ELECTROMAGNETIC EXCITATION OF NUCLEON RESONANCES

Volker D. Burkert
*CEBAF, 12000 Jefferson Avenue, Newport News,
Virginia 23606, USA*

Invited talk presented at the 14th International IUPAP Conference
on Few Body Problems in Physics, 26-31 May 1994, Williamsburg, Va., USA

C E B A F

CONTINUOUS
ELECTRON
BEAM
ACCELERATOR
FACILITY



SURA *Southeastern Universities Research Association*

CEBAF
The Continuous Electron Beam Accelerator Facility

Newport News, Virginia

ELECTROMAGNETIC EXCITATION OF NUCLEON RESONANCES

Volker D. Burkert
*CEBAF, 12000 Jefferson Avenue, Newport News,
Virginia 23606, USA*

ABSTRACT

The status and future prospects of photo- and electroexcitation of nucleon resonances are discussed. Data are compared with calculations within the framework of the constituent quark model. It is shown that measurement of resonance transition amplitudes can be used as a sensitive tool to study the QCD structure of the nucleon.

1. Introduction

Electron scattering off nucleons is described by the familiar one-photon-exchange graph. The properties of the space-like photon are defined by the electron kinematics: the four-momentum transfer $Q^2 = 4EE' \sin^2 \theta_e / 2$, the energy loss of the electron $\nu = E - E'$, and the polarization parameter ϵ . The hadronic cms energy W is given by $W^2 = M^2 + 2M\nu - Q^2$. As ν and Q^2 can be varied independently, the hadronic system can be probed at fixed W and varying Q^2 . Since Q^2 defines the spatial resolution of the probe $\delta r \sim 1/|Q|$, in electroproduction we can probe the transition to a given resonance at different distance scales. At $Q^2 = 0.25 \text{ GeV}^2$ the resolution is about 0.4 fm, while at 4 GeV^2 it is 0.1 fm, allowing us to map out microscopic structure at a distance scale much smaller than the size of the nucleon.

In electron scattering we may identify 3 distinct kinematical regions corresponding to different distance scales. At high energies and small distances the interaction involves elementary quark and gluon fields, acting as quasifree particles. The interaction can be described by perturbative QCD. At the other extreme of interactions at low Q^2 and large distances, quarks and gluons appear in 'condensed' form as nucleons and mesons, and the reaction can be described by hadron theory. At the intermediate distances with which we are concerned, quarks and gluons are relevant, however confinement plays a governing role, and the quarks and gluons appear as constituent quarks and constituent glue, as for example in the flux tube model.¹ This picture, although quite successful in describing many aspects of hadron spectroscopy, is a model whose relationship to QCD remains unclear. Our hope must be that confrontation of detailed predictions of models with accurate data will show where this picture breaks down in non-trivial ways leading to improved models and to a better understanding of the nucleon structure in terms of its fundamental constituents.

In this talk I will use the constituent quark model^{2,3} (CQM) in its various implementations (non-relativistic, relativized) as a guide. It provides physical insight

be shifted, indicating a different Q^2 dependence of the various contributing states. We can therefore expect rich and interesting information about the structure of these states in electron scattering experiments. In order to separate the various resonant states, we must measure the hadronic final states. Which final states are most sensitive to resonance excitations depends on the specific state and its dominant decay channel.

Electromagnetic production of mesons proceeds not only through resonance decays but there are also significant non-resonant contributions one has to take into account in the analysis (Fig. 2). This requires theoretical input which introduces some model dependence into the separation of the resonance contributions. The model dependence can be greatly reduced by measuring several decay channels and by measuring polarization observables, both in the final state and in the initial state. Analysis of the final state hadrons allows the identification of the spin/parity and isospin of the intermediate state, and using information on the hadronic decay vertex we can determine the transverse ($\lambda_{\gamma N} = \frac{1}{2}, \frac{3}{2}$) and scalar ($\lambda_{\gamma N} = \frac{1}{2}$) electromagnetic transition amplitudes $A_{1/2}$, $A_{3/2}$, and $S_{1/2}$ for a given resonance. These are the quantities that can be compared directly to model predictions.

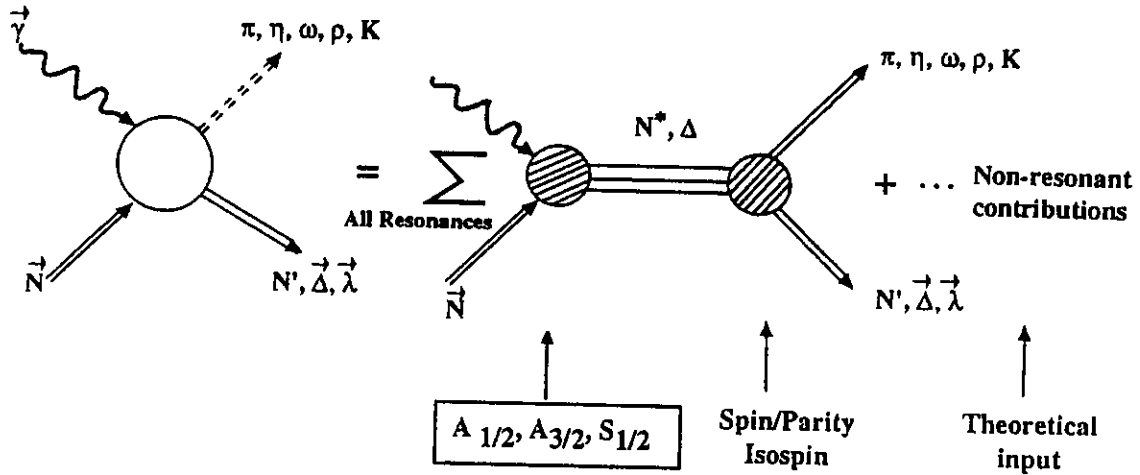


Fig. 2 Analysis of electromagnetic production of mesons

Up until now only single pion and single eta photo- or electroproduction data have been measured and analysed. The differential cross section is given by:

$$\frac{d\sigma}{d\Omega_e dE' d\Omega_\pi} = \Gamma_t [\sigma_t + \epsilon \sigma_l + \epsilon \sigma_{tt} \cos 2\phi + \sqrt{2\epsilon(\epsilon + 1)} \sigma_{lt} \cos \phi] \quad (1)$$

where the σ_i are functions of Q^2 , W , and $\cos \theta^*$. The kinematics for single meson production is shown in Fig. 3.

tions have been made that the missing strength may be due to pion contributions which are not included in the model calculations.

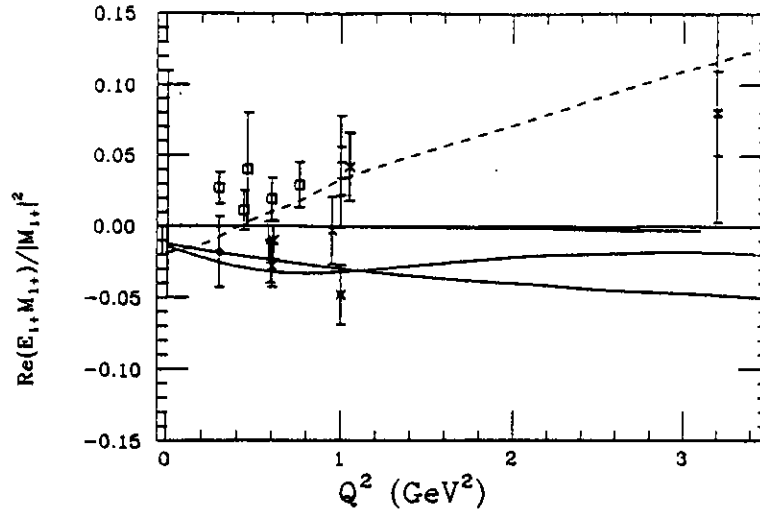


Fig. 4 E_{1+}/M_{1+} for the $\gamma N \Delta(1232)$. The lines correspond to quark model calculations.

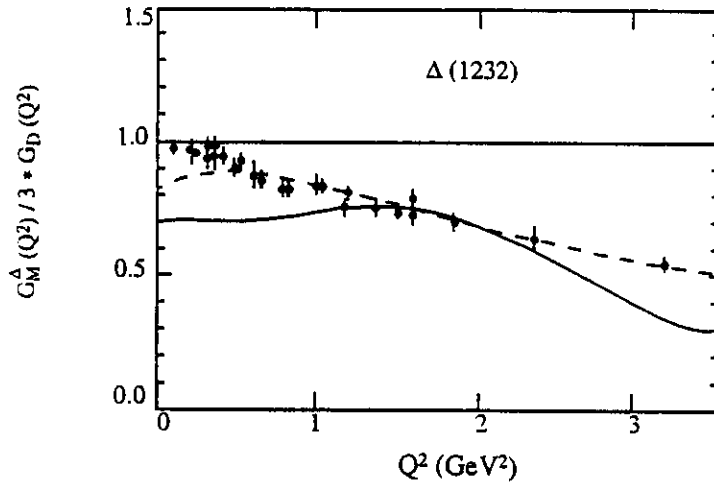


Fig. 5 Magnetic transition form factor $G_M^\Delta(Q^2)$ for the $\gamma N \Delta$ vertex.

3.2. Helicity Switch in $\gamma p \rightarrow D_{13}(1520), F_{15}(1680)$

Radiative transitions to the higher mass states $D_{13}(1520), F_{15}(1680)$ were found to be purely helicity 3/2. In the quark model, this is the result of an accidental cancellation between the spin-flip and the orbit-flip terms. However, in electroproduction

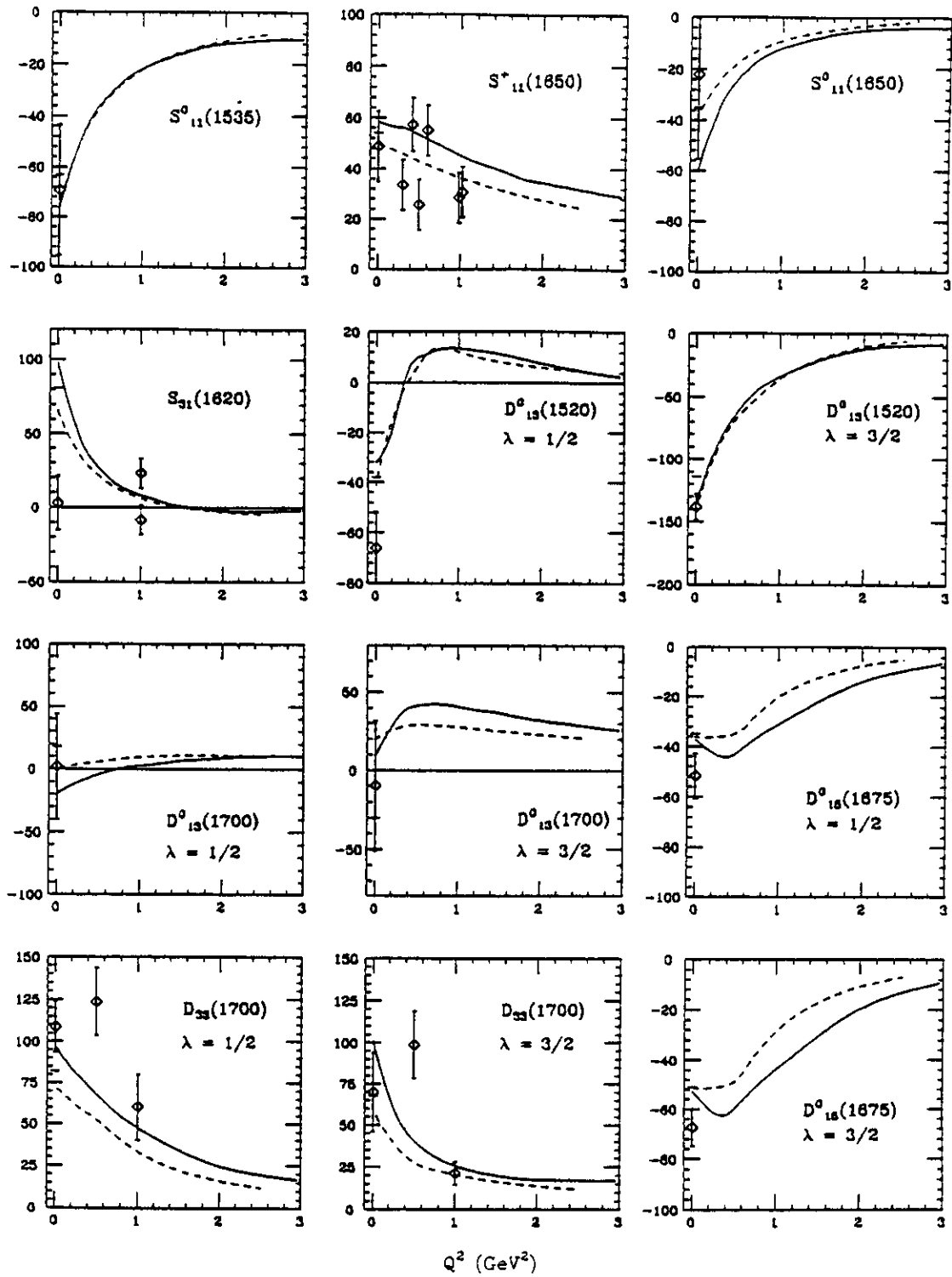


Fig. 8 Predictions of the SQTm for states belonging to the $[70, 1^-]_1$ supermultiplet. The photoproduction data are averages of three independent analyses. The errors are the rms values of the analyses' results. The lines correspond to different parametrizations of the empirical data⁹.

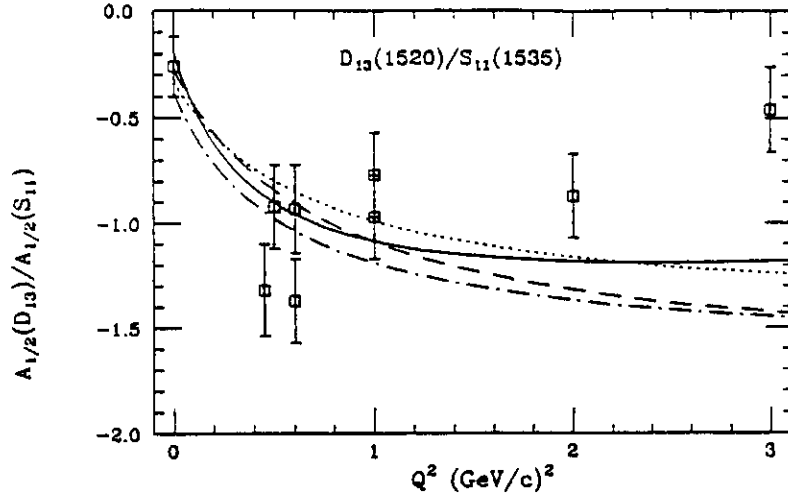


Fig. 9 Test of the constituent quark model symmetry structure. Calculations from ref. [10].

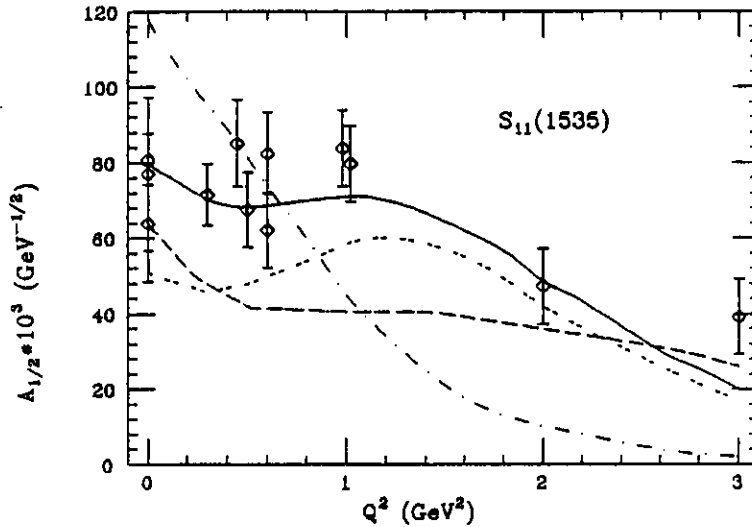


Fig. 10: Transition amplitude for $\gamma_{\nu} p \rightarrow S_{11}^+(1535)$. The lines correspond to quark model calculations: nrCQM - dashed-dotted, rCQM long dashes¹³, solid and double-dashed¹⁴ for different confinement potentials.

effects of the radial wavefunction drop out, and since both states have the same mass, kinematical effects should be minimized. The data are shown in Fig. 9 in comparison with various quark model predictions. The models indicate insensitivity to relativistic effects and other model ingredients. At high Q^2 , the predictions are close to the SU(6) limit for pure spin transitions, which are expected to dominate. While the data agree very well at low Q^2 , the highest Q^2 point indicates a significant deviation. Whether or not this is evidence for a non-trivial breakdown of the CQM at small distances remains to be seen when better and more complete data are available.

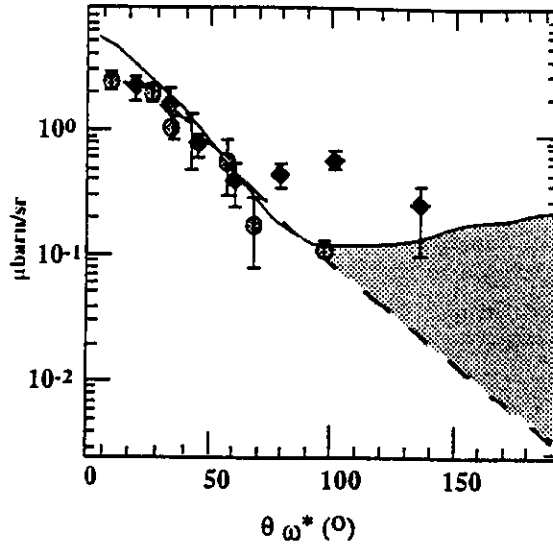


Fig. 12 Search for “missing” quark model states. The dashed line is the expected cross section without resonance contributions, the solid line contains the $F_{15}(1950)$ with the strength as predicted in the nrCQM.

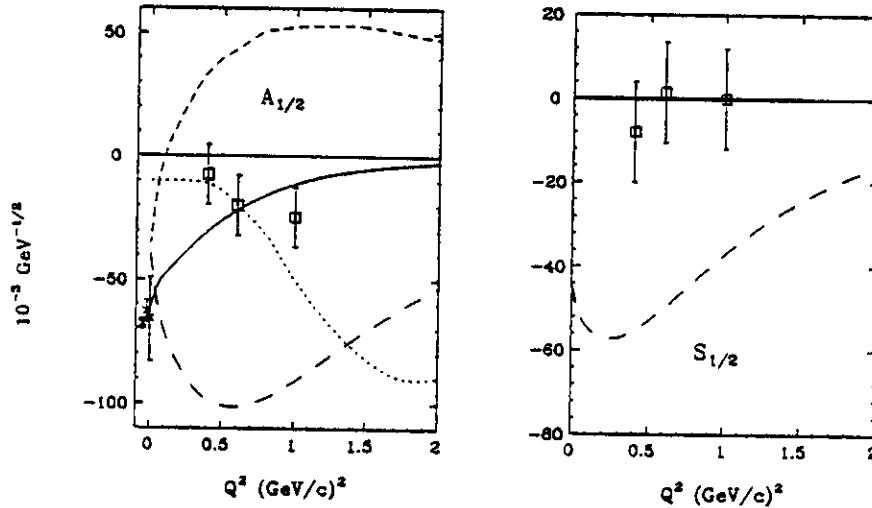


Fig. 13 Transverse and longitudinal transition amplitudes for the $P_{11}(1440)$ for proton targets. The data points represent results of a fixed- t dispersion relation analysis. The broken lines are quark model calculations. The solid lines is the prediction of a q^3G model.

3.7. Electro-Quenching of the $P_{11}(1440)$

In the CQM, the lowest mass $P_{11}(1440)$ state is assigned to a radially excited q^3 state within the $SU(6) \otimes O(3)$ super-multiplet $[56, 0^+]_2$ (i.e. $L_{3Q} = 0$, $N_{3Q} = 2$). However, the observed low mass of the state, as well as the sign and magnitude of the photocoupling amplitudes have traditionally been difficult to reproduce within the framework of the CQM. Moreover, there is experimental evidence that the Q^2 dependence of the photocoupling amplitude $A_{1/2}(Q^2)$ is quite different from what is

also solve a long-standing problem in baryon structure, the strong quenching of the transition form factor $\gamma_p P_{11}(1440)$ with Q^2 .

How can we experimentally discriminate between these alternatives? In a model of the nucleon containing constituent quarks and gluons one graph that is expected to contribute to gluonic excitations is the QCD Compton process $\gamma q \rightarrow Gq$. The inverse process $gq \rightarrow \gamma q$, where g is an elementary gluon, has been studied in detail in hard scattering processes²⁰ and is well described in perturbative QCD. For a gluonic P_{11} , because the gluon has only transverse excitation modes, the longitudinal coupling is absent, $\gamma_{LP} \not\rightarrow P_{11}^G$, and

$$S_{1/2}^G(Q^2) \equiv 0. \quad (6)$$

This is consistent with the analysis of the $P_{11}(1440)$ data, although more accurate data especially at small Q^2 are needed for a more definite comparison.

Precise measurements of $A_{1/2}(Q^2)$ for the $P_{11}(1440)$ could also help discriminate between the interpretation of the $P_{11}(1440)$ as a regular $[56, 0^+]_2 q^3$ state, or as a gluonic excitation where the 3-quark system transforms like a $[70]$ under $SU(6)$. The discriminating power is a result of the fact that the respective photocoupling amplitudes are associated with different spin flavor factors for different spectroscopic assignments, so that in the first approximation (if effects from the spatial wavefunction and relativistic corrections are neglected):

$$\frac{A_{1/2}(P_{11}^G)}{A_{1/2}(P_{11})} \sim \frac{1}{Q^2}. \quad (7)$$

The calculation based on the $q^3 G$ interpretation is in better agreement with the data than calculations using the non-relativistic or relativized versions of the constituent quark model (Fig. 13).

If the $P_{11}(1440)$ is the gluonic partner of the nucleon an interesting question is, what is the mass of the lowest $q^3 P_{11}$? The $P_{11}(1710)$ might be this state. Its mass is also more in accord with the nrCQM estimate. In this case, the photocoupling amplitudes should exhibit a Q^2 dependence characteristic of a radially excited q^3 state.

4. New Generation of N^* Experiments - Lessons from the Past

Study of electro-excitation of N^* resonances in the past has suffered from several shortcomings such as: (1) lack of theoretical guidance, as most measurements were completed in the pre-QCD era when only predictions from simple $SU(6)$ symmetric quark models existed; (2) restriction on single pion production experiments with small solid angle spectrometers, and (3) the complete lack of polarization measurements.

For the single pion (eta) production, the new generation of N^* experiments must aim at precision measurements of at least an order of magnitude improvement in statistical accuracy, as well as detailed measurements of polarization observables. In addition to providing accurate information about states decaying significantly into the $N\pi$, $N\eta$ channels, this will also allow determination of small amplitudes such as E_{1+} , S_{1+} for the $\Delta(1232)$, or the $S_{1/2}$ and $A_{1/2}$ amplitudes for the $P_{11}(1440)$. Measurement of complete angular distributions of the hadronic final states, as well

Table 1. CEBAF Experiments with focus on N^* Physics

Reaction	Physics focus	Q^2 range (GeV^2)	Experiment
$ep \rightarrow e'p\pi^0$ $ep \rightarrow e'n\pi^+$ $ed \rightarrow e'p\pi^-p_s$ $\bar{e}p \rightarrow e'p\pi^0$ $\bar{e}p \rightarrow e'n\pi^+$ $\bar{e}p \rightarrow e'\bar{p}\pi^0$ $\bar{e}\bar{p} \rightarrow e'p\pi^0$ $\bar{e}\bar{p} \rightarrow e'n\pi^+$	$\Delta(1232)$ Model independent determination of multipoles M_{1+}, E_{1+}, S_{1+} , in large Q^2 range	≤ 4 4 ≤ 3 ≤ 4 ≤ 2 ≤ 2 1 ≤ 4 ≤ 4	E-89-037 ²² /40 ²³ E-94-014 ²⁴ E-89-037 E-89-037 E-89-042 ²⁵ E-89-042 E-91-011 ²⁶ PR-94-003 ²⁷ PR-94-003
$ep \rightarrow e'p\pi^0$ $ep \rightarrow e'n\pi^+$ $ed \rightarrow e'p\pi^-p_s$ $\bar{e}p \rightarrow e'p\pi^0$ $\bar{e}\bar{p} \rightarrow e'n\pi^+$	$P_{11}(1440), D_{13}(1520), F_{15}(1680)$ Transition amplitudes in large Q^2 range, gluonic baryons	≤ 3 ≤ 4 ≤ 4 ≤ 2 ≤ 2	E-89-038 ²⁸ E-89-038 E-89-038 E-93-036 ²⁹ E-93-036
$ep \rightarrow e'N\pi\pi$ ($\Delta\pi, N\rho$)	$S_{31}(1620), D_{33}(1700), D_{15}(1700)$ Precise tests of the SQTm Missing q^3 states, $I = 1/2, 3/2$	≤ 2	E-93-006 ³⁰
$ep \rightarrow e'p\omega$	Missing q^3 states with $I = 1/2$	≤ 1	E-91-024 ³¹
$ep \rightarrow e'p\eta$	$S_{11}(1535), P_{11}(1710)$ Transition form factors	≤ 4	E-89-039 ³² /040
$ep \rightarrow e'\Delta^{++}\pi_{soft}^-$	$G_A^\Delta(Q^2)$, Axial vector transition form factors to Δ	≤ 3	E-94-005 ³³
$\gamma p \rightarrow \eta p$ $\gamma p \rightarrow \eta' p$	$S_{11}(1535), P_{11}(1710)$ Photocoupling amplitudes, gluonic baryons	0 0	E-91-008 ³⁴ E-91-008
$\gamma p \rightarrow p\pi^+\pi^-$	Missing q^3 states, $I = 1/2, 3/2$	0	E-93-033 ³⁵

The reactions $ep \rightarrow ep\eta$, $\gamma p \rightarrow p\eta$ will be used to study the $S_{11}(1535)$ and $P_{11}(1710)$ states, and to search for other isospin 1/2 excitations. The $\gamma p \rightarrow p\eta'$ reaction may be sensitive to gluonic baryon excitations at higher masses.

Most of the experimental studies of N^* transitions have focussed on the vector structure of the hadronic current. Very little is known experimentally about the axial vector structure and the corresponding axial vector transition form factors for excited states. Direct access to these form factors can be obtained in neutrino scattering experiments. However, it is very difficult in these experiments to obtain the statistics required for a complete partial wave analysis of the reaction. Therefore alternative methods to get access to the axial structure have long been sought for. Alternative reactions in electroproduction of resonances in coincidence with an additional pion have been suggested as an alternative process. For example, the process

$$ep \rightarrow e'\Delta^{++}\pi_{soft}^-$$

where the π^- is produced near threshold, appears to be an attractive alternative method for measuring the axial vector transition form factor G_A^Δ from the nucleon to the $\Delta(1232)$. Threshold pion production can be related to the axial vector current using current algebra and the PCAC theorem³⁷. In terms of Feynman diagrams, threshold production is directly related to the 'contact' interaction with the vertex $\gamma_\nu p \Delta \pi$. A proposal to measure $\Delta^{++}\pi^-$ production near threshold has just been approved for CEBAF.³³ The projected accuracy for $G_A^\Delta(Q^2)$ from this measurement is shown in Fig. 16.

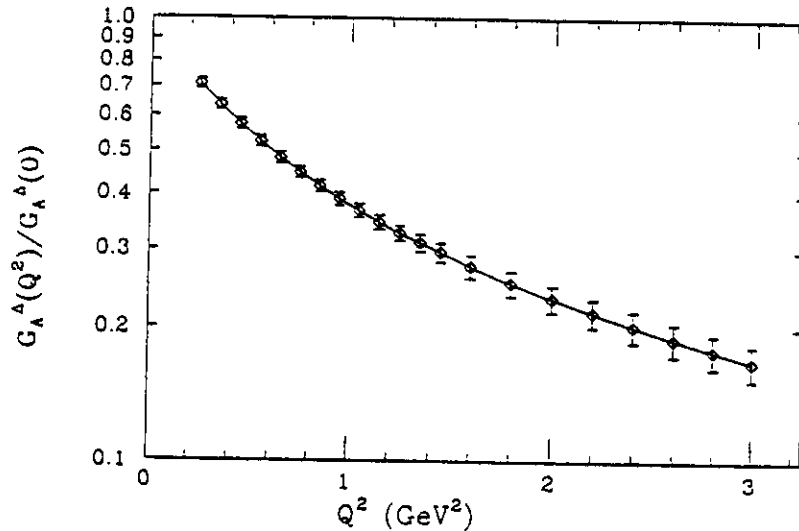


Fig. 16 Projected error bars for a measurement of the axial vector transition form factor from the nucleon to the $\Delta(1232)$.

24. J. Napolitano, P. Stoler, et. al., *CEBAF Experiment E-94-014*
25. V. Burkert, R. Minehart, et. al., *CEBAF Experiment E-89-42*
26. R. Lourie, et. al., *CEBAF Experiment E-91-011*
27. P. Stoler, V. Burkert, Zh. Li, R. Minehart, et. al., *CEBAF Proposal PR-94-003*
(conditionally approved)
28. R. Minehart, V. Burkert, M. Gai, et. al., *CEBAF Experiment E-89-038*
29. H. Weller, R. Chasteler, R. Minehart, et. al., *CEBAF Experiment E-93-036*
30. M. Ripani, V. Burkert, et. al., *CEBAF Experiment E-93-006*; see also: M. Ripani and V. Burkert, *Proceedings, Workshop on "Exclusive Reactions at High Momentum Transfer", Elba, Italy, July 1993*
31. H. Funsten, V. Burkert, M. Manley, B. Mecking et al., *CEBAF Experiment E-91-024*
32. S. Dytman, K. Giovanetti, et. al., *CEBAF Experiment E-89-039*
33. L. Elouadrhiri, D. Heddle, R. Hicks, Zh. Li, et. al., *CEBAF Experiment E-94-005*
34. B. Ritchie, et. al., *CEBAF Experiment E-91-008*
35. J. Napolitano et. al., *CEBAF Experiment E-93-033*
36. P. Bertin et. al., *CEBAF Experiment E-93-050*
37. S. Adler and W. Weisberger, *Phys. Rev.* 169, 1392 (1968)